

2D/3D image charge for modeling field emission

Kevin L. Jensen, Donald A. Shiffler, John R. Harris, Ian M. Rittersdorf, and John J. Petillo

Citation: Journal of Vacuum Science & Technology B 35, 02C101 (2017); doi: 10.1116/1.4968007

View online: http://dx.doi.org/10.1116/1.4968007

View Table of Contents: http://scitation.aip.org/content/avs/journal/jvstb/35/2?ver=pdfcov Published by the AVS: Science & Technology of Materials, Interfaces, and Processing

Articles you may be interested in

Exfoliated 2D black phosphorus nanosheets: Field emission studies J. Vac. Sci. Technol. B **34**, 041803 (2016); 10.1116/1.4945433

Enhanced field emission properties from oxygen-deficient α-Fe2O3 nanorod arrays

J. Vac. Sci. Technol. B 34, 021803 (2016); 10.1116/1.4942006

Molecular dynamics simulations of field emission from a planar nanodiode

Phys. Plasmas 22, 033109 (2015); 10.1063/1.4914855

A relativistic self-consistent model for studying enhancement of space charge limited field emission due to counter-streaming ions

Phys. Plasmas 21, 023118 (2014); 10.1063/1.4866601

Space charge effects in field emission: One dimensional theory

J. Appl. Phys. 107, 014904 (2010); 10.1063/1.3272690





2D/3D image charge for modeling field emission

Kevin L. Jensen^{a)}

Naval Research Laboratory, Washington, DC 20375

Donald A. Shiffler and John R. Harris

Air Force Research Laboratory, Albuquerque, New Mexico 87117

Ian M. Rittersdorf

Naval Research Laboratory, Washington, DC 20375

John J. Petillo

Leidos Corp., Billerica, Massachusetts 01821

(Received 15 September 2016; accepted 3 November 2016; published 21 November 2016)

Analytic image charge approximations exist for planar and spherical metal surfaces but approximations for more complex geometries, such as the conical and wirelike structures characteristic of field emitters, are lacking. Such models are the basis for the evaluation of Schottky lowering factors in equations for current density. The development of a multidimensional image charge approximation, useful for a general thermal-field emission equation used in space charge studies, is given and based on an analytical model using a prolate spheroidal geometry. A description of how the model may be adapted to be used with a line charge model appropriate for carbon nanotube and carbon fiber field emitters is discussed. [http://dx.doi.org/10.1116/1.4968007]

I. INTRODUCTION

High brightness field emission sources in an array (either conical Spindt-like or long wirelike as in carbon fibers and nanotubes) may provide electron beams that meet the needs of accelerators, high power microwave and x-ray sources, and vacuum electronic devices. With very high current per emitter, emitted charge complicates the simulation of space charge affected field emission, ^{1,2} particularly in beam optics codes.³ It is common to account for Schottky barrier lowering $\Delta\Phi$ under the presumption of a planar image charge modification, or $\Delta \Phi = \sqrt{4QF}$, where $Q = q^2/16\pi\varepsilon_0 = 0.36 \,\mathrm{eV}$ nm and $F = q\mathcal{E}$: in the image charge formula, the electric field \mathcal{E} always appears with the electron charge -q. The convention here is to use $F \equiv q\mathcal{E}$ with units of (eV/nm). Although a force, F will nevertheless be referred to by its colloquial usage of "field" insofar as F in (eV/nm) is numerically equal to \mathcal{E} in (GV/m). Units and conventions will therefore follow Refs. 4 and 5.

Unit cell models under development for particle-in-cell codes which treat a single emitter unit, as well as field emission in small AK gaps and emission from nanoprotrusions and/or wirelike emitters such as carbon nanotubes (CNTs) and carbon fibers, have configurations for which the planar image charge approximation requires modification, particularly when tunneling calculations rely on actual paths in multidimensions rather than simplified linear fields in one dimension. In the present study, we describe the development of a multidimensional image charge approximation useful for a general thermal-field emission equation used in space charge studies based on an analytical model using a prolate spheroidal geometry. We shall describe a model that may be adapted to be used with a line charge model appropriate for CNT and carbon fiber field emitters, itself a generalization

II. SPHERICAL IMAGE CHARGE APPROXIMATION

Even for field emitters for which the apex is on the order of 10 nm, ^{16,17} a common method to find total current is to integrate the local current density J(F) over the surface element $d\Omega$ of an emitter^{5,18} using the planar-based Fowler–Nordheim equation which in turn is dependent on the planar image charge model of the barrier. A simple correction to accommodate curvature effects into the estimate of total current is to incorporate the image charge associated with a hemispherical shape (a staple boundary value problem in electrodynamics textbooks^{19,20} and elsewhere^{5,21}) characterized by a tip radius a, by redefining the work function by $\Phi_a = \Phi + (Q/2a)$ in the Fowler-Nordheim equation^{5,22} (although important, the modifications to the transmission probability accounting for trajectory curvature effects which increase the tunneling barrier an electron encounters are not part of the present analysis, although they can be included 10,23,24). The changes wrought on $J(F) = (A/\Phi t(y)^2)F^2 \exp(-B\Phi^{3/2}/F)$ as commonly used, where $A = (16\pi^2\hbar)^{-1}$ and $B = (4/3\hbar)\sqrt{2m}$ are as follows for the simple model. Using the Forbes-Deane approximation to the "Schottky-Nordheim barrier functions" v(y) and t(y), 25 then the oft-used Murphy and Good form of the Fowler–Nordheim compactly becomes ¹⁰

$$J_{FN}(F) \to \tilde{A}F^{2-\nu} \exp\left(-B\frac{\Phi^{3/2}}{F}\right),$$
 (1)

of point and line segment charge models that can be used to model field emitters. The elongation of the emitter will be seen to affect quite strongly the simple form of the spherical image charge, but as emission is concentrated on axis, the form developed herein is expected to provide a reasonable account of the nonplanar image charge effects. The model is developed by analogy to a common model of the image charge for an electron outside a spherical surface.

a)Electronic mail: kevin.jensen@nrl.navy.mil

through the introduction of the parameters ν and \tilde{A} defined by

$$\nu \equiv \frac{8Q}{9\hbar} \sqrt{\frac{2m}{\Phi}}; \quad \tilde{A} \equiv \frac{A}{t_o^2} \left(\frac{e^6}{4Q}\right)^{\nu} \Phi^{2\nu - 1}, \tag{2}$$

where $y_o = e^{-1/2}$ so that $t(y_o) = 1 + (e^1/6) = 1.0613$. Consequently, the hemispherical image charge affects the usual argument of the exponential term [the slope of $\ln(J/F^2)$ as a function of 1/F in the Fowler–Nordheim representation of data] but also the power that F is raised to in the coefficient $(2 - \nu)$ and the intercept \tilde{A} .

Finding image charge modification departures from the hemispherical result will be accomplished as follows. First, the derivation of the image charge for a sphere shall be compactly given. Second, the same methods shall then be applied to a prolate spheroidal model of an emitter tip.

Solving for the image charge associated with a point charge outside a sphere can make usage of Legendre polynomial expansions, ¹⁹ but a more straightforward method is as follows. The origin is taken as the center of the sphere. The image charge is placed so that it satisfies the boundary conditions, which constitutes a unique and valid solution to the electrostatic problem. To ensure that the surface of the rounded hemisphere is at zero potential, the potential due to the external charge located a distance d from the origin is $V(\vec{r}_2) = 4Q/r_2$, which is set equal to the potential of the image charge $V(\vec{r}_1) = 4\lambda Q/r_1$ located a distance d' from the origin along the axis defined by the origin (center of sphere) and the location of the external charge -q. Also, λ is a dimensionless number, on the surface of the sphere where $|\vec{r}| = a$. Using the notation of Fig. 1, then the problem is equivalent to

$$\frac{4^2}{a^2 + d^2 - 2ad\cos\theta} = \frac{(4\lambda)^2}{a^2 + dt^2 - 2ad'\cos\theta}.$$
 (3)

Rewriting the left hand side (LHS) as

LHS =
$$\frac{1}{(a^2 + d^2) \left[1 - \frac{2ad}{a^2 + d^2} \cos \theta \right]}$$
, (4)

and setting it equal to the right hand side (RHS) expressed as

RHS =
$$\frac{\lambda^2}{(a^2 + dt^2) \left[1 - \frac{2ad'}{a^2 + d'^2} \cos \theta \right]}$$
 (5)

quickly demonstrates that the assignments

$$d' = \frac{a^2}{d}; \quad \lambda = \left(\frac{a^2 + d'^2}{a^2 + d^2}\right)^{1/2} = \frac{a}{d},\tag{6}$$

ensure that LHS = RHS. To a charge a distance (d-a) from the surface of the sphere, the potential energy of its interaction with the image charge is then found by evaluating $V_i = 4\lambda Q/(d-a+(a-d')) = 4aQ/(d^2-a^2)$. With the replacement $d \rightarrow r$ as the distance of the charge from the center of the

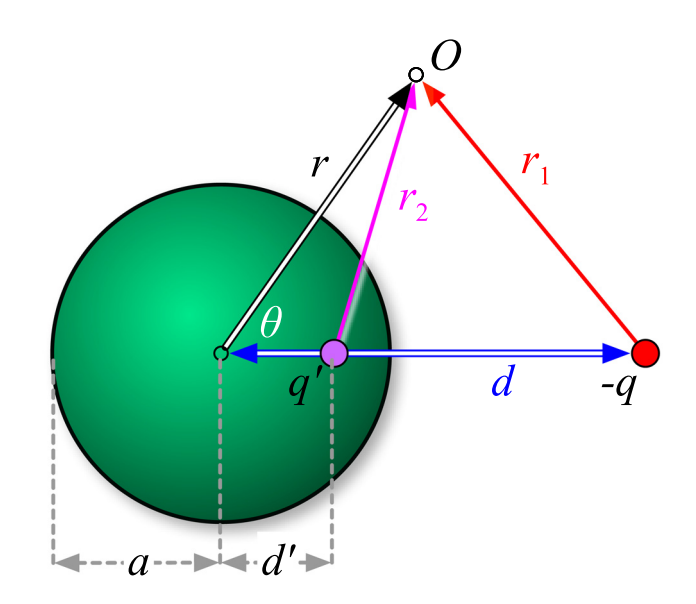


Fig. 1. (Color online) External charge -q is at a distance d (horizontal double-lined arrow) from the center of a sphere of radius a, and its image charge q' that results at a distance d' from the sphere center. \vec{r}_1 is the distance to the observation point O from the external charge; \vec{r}_2 is the distance to the observation point from the image charge. The origin of the coordinate system is the center of the sphere (r=0).

sphere, the conventional form $V_i(r) = 4aQ/(r^2 - a^2)$ results. Letting r = a + x for x small then regains the modifications to Φ discussed in Sec. II accounting for curvature.

III. PROLATE SPHEROIDAL GEOMETRY

Prolate spheroidal coordinate systems are an orthogonal coordinate system well-suited to modeling hyperbolic (diode) or ellipsoidal (needle in field) models of field emitters. They can give analytic field enhancement and emission area factors⁵ in a straightforward manner. The advantage here is that in prolate spheroidal coordinates, surfaces of emitters correspond to one of the coordinates, and field lines to the other in a manner suggested in Fig. 2. Because the analog of two parallel plates is one anode plate and a curved emitter, the hyperbolic coordinates are used, in terms of which the cylindrical variables (z, ρ) are

$$\rho(\alpha, \beta) = L \sinh \alpha \sin \beta, \tag{7}$$

$$z(\alpha, \beta) = L \cosh \alpha \cos \beta, \tag{8}$$

where L establishes the length scale. The prolate spheroidal coordinates are therefore governed by (α, β) .

Due to rotational symmetry, *rings* of charge are emitted from the field emitter, and the image of a ring is what shall be found. A cross-section of the geometry is shown in Fig. 3, but the "points" should be understood to rings when the figure is rotated about the \hat{z} -axis. A subscript "s" (for "source") on (z, ρ) shall denote the specification of the emitted ring of charge, and likewise, a subscript "i" (for "image") denotes the image ring inside the tip. A subscript of "o" denotes the surface of the emitter.

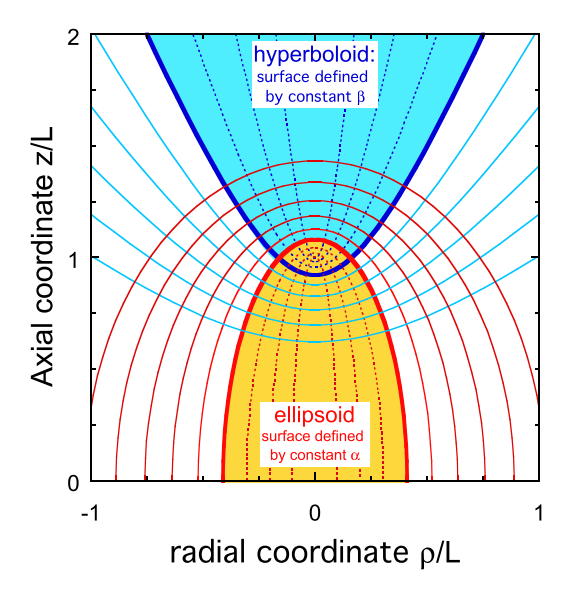


Fig. 2. (Color online) Coordinates of a prolate spheroidal geometry. The surface is given by a hyperboloid of revolution; the field lines follow the ellipsoids.

In the rotationally symmetric problem, rings of charge are now characterized by a λ which is the charge per unit length. The potential $V_s(\rho_s, z_s)$ due to the source ring is

$$V_s = \frac{2\lambda_s Q}{\pi} \int_0^{2\pi} \frac{d\phi}{\left[r^2 + \rho_s^2 - 2r\rho_s \sin\theta_s \cos\phi\right]^{1/2}},\tag{9}$$

whereas the potential $V_i(\rho_i, z_i)$ due to a ring is

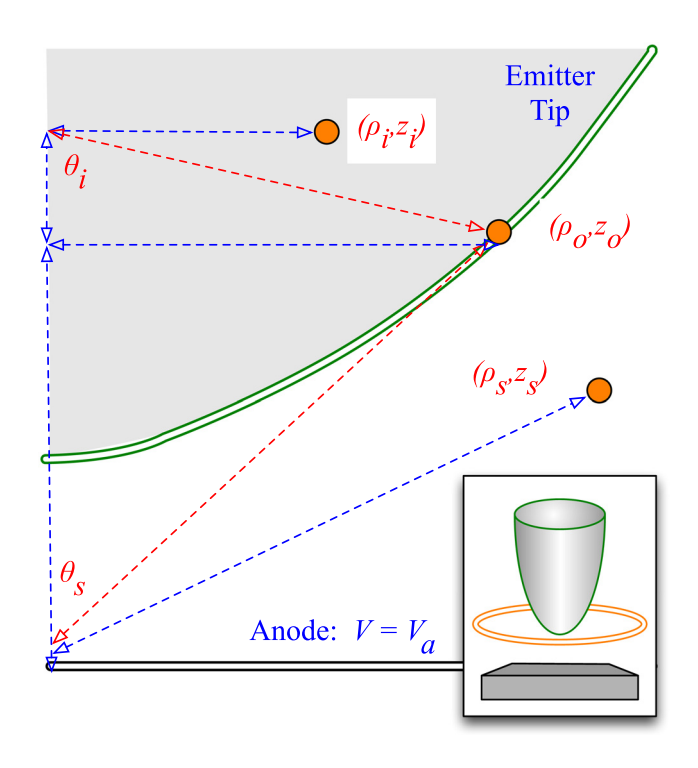


Fig. 3. (Color online) Specification of the image ring and its location in (ρ, z) coordinates. The inset on the lower right shows a 3D image of how a ring of emitted charge may appear in relation to the tip and the anode plane.

$$V_i = \frac{2\lambda_i Q}{\pi} \int_0^{2\pi} \frac{d\phi}{\left[r^2 + \rho_i^2 - 2r\rho_i \sin\theta_i \cos\phi\right]^{1/2}},\tag{10}$$

where ϕ is the azimuthal coordinate in cylindrical coordinates. The z-coordinate of the rings is momentarily hidden in the usage of the radial r^2 term for brevity, instead of expanding out the expression in only cylindrical coordinates. As with the spherical case, $V_i + V_s = 0$ along the surface ($z = z_o$, $\rho = \rho_o$), for which the distances from the rings to the observation ring are given by, where now the presence of z is restored to its rightful place,

$$r_o^2 = \rho_o^2 + (z_o - z_s)^2,$$

$$r_i^2 = \rho_o^2 + (z_i - z_o)^2.$$
(11)

Setting $V_s = V_i$ as with the spherical case, but after eliminating common factors and simplifying the relations using trigonometric half-angle formulae, then

$$V_{s} = \frac{\lambda_{s}}{h_{s}} \int_{0}^{2\pi} \frac{d\phi}{\left\{1 + \frac{\rho_{o}\rho_{s}}{h_{s}^{2}} \sin^{2}(\phi/2)\right\}^{1/2}},$$
(12)

$$V_{i} = \frac{\lambda_{i}}{h_{i}} \int_{0}^{2\pi} \frac{d\phi}{\left\{1 + \frac{\rho_{o}\rho_{i}}{h_{i}^{2}} \sin^{2}(\phi/2)\right\}^{1/2}},$$
(13)

where integrations are required to sum over all the small differential elements of the rings, and where the h-factors are introduced and defined by

$$h_s^2 = (\rho_s - \rho_o)^2 - (z_s - z_o)^2,$$

$$h_s^2 = (\rho_o - \rho_i)^2 - (z_o - z_i)^2.$$
(14)

Three unknowns exist, λ_i = the charge on the ring, ρ_i = the radius of the ring, and z_i = the height of the ring. As a consequence, three relations are required to specify them uniquely. The relations, required to ensure the equivalence of Eqs. (12) and (13) in a manner analogous to Eq. (3), are

- (1) Field lines: (ρ_s, z_s) and (ρ_i, z_i) lie on same arc;
- (2) Charge: $\lambda_s/h_s = \lambda_i/h_i$; and
- (3) Ring: $\rho_o \rho_s / h_s^2 = \rho_o \rho_i / h_i^2$.

For relation (1), in a hyperbolic (prolate spheroidal) system, the field lines are lines of constant α , or

$$\rho_x = L \sinh \alpha_o \sin \beta_x,$$

$$z_x = L \cosh \alpha_o \cos \beta_x,$$
(15)

for x = o (surface), s (emitted ring), or i (image ring). The h-factors are then

$$h_s^2 = L^2 \sinh^2 \alpha_o (\sin \beta_s - \sin \beta_o)^2 + L^2 \cosh^2 \alpha_o (\cos \beta_o - \cos \beta_s)^2,$$
 (16)

$$h_i^2 = L^2 \sinh^2 \alpha_o (\sin \beta_o - \sin \beta_i)^2 + L^2 \cosh^2 \alpha_o (\cos \beta_i - \cos \beta_o)^2.$$
 (17)

For relation (2), relation (3) entails $h_i/h_s = \sqrt{\rho_i/\rho_s}$; therefore, it follows

$$\lambda_i = \lambda_s \left(\frac{\sin \beta_i}{\sin \beta_s} \right)^{1/2}. \tag{18}$$

Finally, relation (3) becomes

$$\frac{\sin \beta_i}{(\sin \beta_i - \sin \beta_o)^2 \tanh^2 \alpha_o + (\cos \beta_i - \cos \beta_o)^2}$$

$$= \frac{\sin \beta_s}{(\sin \beta_s - \sin \beta_o)^2 \tanh^2 \alpha_o + (\cos \beta_o - \cos \beta_o)^2},$$
(19)

from which $\beta_i(\alpha_o, \beta_o, \beta_s)$ can be evaluated. As a result, the location (ρ_i, z_i) of the image ring and the and magnitude (λ_i) of its charge can be found by numerical means.

The actual utilization of the ring image charge model requires adaptations that will be reported separately, related primarily to how to use the ring image charge in numerical simulations in a computationally efficacious manner. The image charge associated with the ring will change as a consequence of two changes. The first change is to λ_i : because it will decrease the associated Schottky-barrier-like reduction factor, the barrier height will increase. The second change is the evaluation of the WKB tunneling factor (alternately called the Gamow factor) $\theta(k)$, which increases because the integration leading to $\theta(k)$ for the tunneling barrier follows an arc rather than a straight line⁷ and can be modeled by a quadratic term in the potential $V(x) = \mu + \Phi - Fx - Q/x + \gamma x^2$, with the standard image charge potential resulting in the $\gamma \to 0$ limit.²³ Additionally, space charge will complicate the determination of the surface field.²⁶ As a result of such effects, a change in the emission probability will result. These effects will be taken up separately. Here, a demonstration of the asymptotic relations is given instead. Consider, therefore, two limiting cases of Eq. (19) in terms of β_o , namely, flat and very sharp geometries. To those ends, let $\beta_s = \beta_o + \delta$ and $\beta_i = \beta_o - \epsilon$, where δ and ϵ are both small. From Eq. (19)

$$\frac{\tan \beta_o + \delta}{\delta^2} = \frac{\tan \beta_o - \epsilon}{\epsilon^2}.$$
 (20)

When δ and ϵ are both small, then

$$\beta_o - \beta_i \approx \frac{(\beta_s - \beta_o) \tan \beta_o}{\beta_s - \beta_o + \tan \beta_o}.$$
 (21)

The two limiting cases are then as follows:

(1) Flat cathode: When $\beta_o \to \pi/2$, then $\tan \beta_o \to \infty$. The parallel plate result is then recovered: the image ring is as far from the surface (β_o) as the emitted ring and so $\epsilon = \delta$, as known from the usual planar image charge model.

(2) Sharp tip: When β_o is small, then $\tan \beta_o \approx \beta_o$ and $\epsilon = \beta_o \delta/(\beta_o + \delta)$. Alternately, if $\delta = \beta_o/n$, then $\epsilon = \beta_o/(n+1)$. This entails that a ring of emitted charge located just outside the surface for which $(\beta_s \approx \beta_o)$, results in an image charge ring at $\beta_o/2$, and the image ring is fixed in location by geometry.

IV. CONCLUSION

Modeling field emission from the apex of a protrusion requires the evaluation of the WKB tunneling factor based on an image charge representation. The WKB factor is affected by curvature of the trajectory lines resulting in a suppression of emission down the sides of the emitter tip;⁷ the effect on current has been found previously for prolate spheroidal geometries. In this work, a different effect due to the change of the image charge potential due to the prolate spheroidal geometry is considered. Rotational symmetry of the problem renders the evaluation most conveniently expressed as the image of a ring of charge emitted from the tip. The charge of the image ring has been derived, and its magnitude λ_i and position (ρ_i, z_i) have been determined. From this, potentials and forces from the ring of charge can be found everywhere, and therefore, the modifications entailed for a general thermal-field emission model can be obtained. Of most interest for future work is the impact of the ring image charges on space charge effects in field emission, 1,2,8 as some of the source rings will be below the emitter apex with an unusual impact expected on the particle dynamics. Space charge limited flow near the apex of a prolate spheroidal geometry can exceed the usual 1D Child's law limit because trajectories have the opportunity to move away from the symmetry axis, 8,26 even while the potential barrier itself becomes less favorable to emission. The complexity of space charge and image charge modified field emission is therefore substantially greater than the corresponding 1D treatments. The intended application of the models described herein are for beam optics codes³ used to treat space charge affected field emission in real devices. The next step is to develop a modified tip current model accounting for the effects of prolate spheroidal geometries on total current per tip models in a manner analogous to previous efforts using the planar image charge approximation. ¹⁰

ACKNOWLEDGMENTS

The authors gratefully acknowledge support from J. Luginsland and J. Marshal, *Air Force Office of Scientific Research* (AFOSR).

¹R. Forbes, J. Appl. Phys. **104**, 084303 (2008).

²A. Rokhlenko, K. L. Jensen, and J. L. Lebowitz, J. Appl. Phys. **107**, 014904 (2010).

³J. J. Petillo, D. N. Panagos, and K. L. Jensen, *Proceedings of the IEEE International Vacuum Electronics Conference IVEC* (2014), pp. 79–80. ⁴K. L. Jensen, Ultramicroscopy **95**, 29 (2003).

⁵K. L. Jensen, Wiley Encyclopedia of Electrical and Electronics

Engineering, edited by J. G. Webster (Wiley, New York, 2014). ⁶P. Kapur and R. Peierls, Proc. R. Soc. London, Ser. A **163**, 0606 (1937).

⁷A. Kyritsakis, G. Kokkorakis, J. Xanthakis, T. Kirk, and D. Pescia, Appl. Phys. Lett. **97**, 023104 (2010).

- ⁸K. L. Jensen, D. A. Shiffler, I. M. Rittersdorf, J. L. Lebowitz, J. R. Harris, Y. Y. Lau, J. J. Petillo, W. Tang, and J. W. Luginsland, J. Appl. Phys. 117,
- ⁹K. L. Jensen, J. Vac. Sci. Technol., B **21**, 1528 (2003).
- 10 K. L. Jensen, D. A. Shiffler, J. J. Petillo, Z. Pan, and J. W. Luginsland, Phys. Rev. Spec. Top.-Accel. Beams 17, 043402 (2014).
- ¹¹D. A. Shiffler, W. Tang, K. L. Jensen, K. Golby, M. LaCour, J. J. Petillo, and J. R. Harris, J. Appl. Phys. 118, 083302 (2015).
- ¹²J. Harris, K. Jensen, and D. Shiffler, J. Phys. D: Appl. Phys. **48**, 385203 (2015).
- ¹³G. Mesa, E. DobadoFuentes, and J. Saenz, J. Appl. Phys. **79**, 39 (1996).
- ¹⁴K. L. Jensen, Y. Y. Lau, D. W. Feldman, and P. G. O'Shea, Phys. Rev. Spec. Top.-Accel. Beams 11, 081001 (2008).

 15 A. C. Keser, T. M. Antonsen, G. S. Nusinovich, D. G. Kashyn, and K.
- L. Jensen, Phys. Rev. Spec. Top.-Accel. Beams 16, 092001 (2013).
- ¹⁶C. A. Spindt, I. Brodie, L. Humphrey, and E. R. Westerberg, J. Appl. Phys. 47, 5248 (1976).

- ¹⁷P. R. Schwoebel, C. A. Spindt, and C. Holland, J. Vac. Sci. Technol., B 23, 691 (2005).
- ¹⁸R. Hartman, W. Mackie, and P. Davis, J. Vac. Sci. Technol., B 12, 754 (1994).
- ¹⁹L. Eyges, The Classical Electromagnetic Field (Addison-Wesley, Reading, MA, 1972).
- $^{20}\mathrm{J}.$ D. Jackson, Classical Electrodynamics (Wiley, New York, 1975).
- ²¹R. G. Forbes, C. J. Edgcombe, and U. Valdre, Ultramicroscopy **95**, 57
- ²²K. L. Jensen and E. G. Zaidman, Appl. Phys. Lett. **63**, 702 (1993).
- ²³K. L. Jensen, D. W. Feldman, and P. G. O'Shea, J. Vac. Sci. Technol., B 23, 621 (2005).
- ²⁴A. Kyritsakis and J. P. Xanthakis, Proc. R. Soc. London, A **471**, 20140811 (2015).
- ²⁵J. H. B. Deane and R. G. Forbes, J. Phys. A **41**, 395301 (2008).
- ²⁶Y. B. Zhu and L. K. Ang, Phys. Plasmas **22**, 052106 (2015).